

Photometry of the solar corona of March 7, 1970

M K V BAPPU, J C BHATTACHARYYA and K R SIVARAMAN
Indian Institute of Astrophysics, Kodaikanal and Bangalore

MS received 5 June 1973

Abstract. Isophotes obtained by equidensitometry techniques from four exposures of the March 7, 1970 corona are used for derivation of intensity distributions along the equator, poles, streamers and dark 'gaps' in the visible corona. The distributions differ from the van de Hulst curves for a maximum corona. The Kodaikanal measures agree well with the NRL measures of the outer corona made from a rocket coronagraph and together provide data from $1.2R_{\odot}$ to $8.0R_{\odot}$ along the solar equator. Radial intensity gradients for different position angles and the Ludendorff parameters obtained, characterize this corona as typical of the solar maximum.

Keywords. Solar corona; solar eclipse; coronal photometry.

1. Introduction

A two-member team was sponsored by the Kodaikanal Observatory to carry out a programme of spectrophotometry of the emission corona and wideband high resolution photometry of coronal form and intensity. The experiments planned were the simultaneous spectroscopy of the corona at the east and west limbs in the spectral range $3200\text{Å} - 8800\text{Å}$, as well as direct photography of the corona with two cameras of focal lengths 1.2 metres and 6.0 metres. The eclipse camp was set up in the outskirts of the small town of Miahuatlan (latitude $16^{\circ} 18' 50''$ N, longitude $90^{\circ} 35' 44''$ W, altitude 1607 metres), about 20 kilometres north of the central line of totality. The duration of totality at this site was 203.5 seconds. Second contact was predicted to be at $17^{\text{h}} 28^{\text{m}} 56.4$ U.T. or local time $11^{\text{h}} 28^{\text{m}}$ with the sun high up in the sky a half hour before noon. Eclipse day had blue skies of very high transparency. The air was calm around totality and thus the conditions for observation of a total eclipse of the sun were remarkably exceptional.

2. The observations

Two experimental arrangements for wide band photography provided the data for coronal photometry. The first utilized the 6.0 metre camera working at $f/48$ in a horizontal arrangement with sunlight fed by a two mirror coelostat of 30 cm aperture. The focal plane end of the closed camera tube was enclosed in an observation hut where one of the observers was stationed. Six exposures could be taken with this camera with

Table 1. Details of exposure of the coronal photographs

Plate No.	Mid-epoch of exposure U.T.	Duration (sec)	Developer used	Isophotes derived
I	17 28 58	1	D-19	—
II	17 29 17	11	Promicrol	19-23*
III	17 29 49	30	Microdol	15-18
IV	17 30 43	50	Promicrol	10-14
V	17 31 29	17	Promicrol	1- 9

*Isophote 23 is the innermost one

the aid of a rotating plate holder that accommodated 8×10 inch plates. The shutter of the camera located in front of the 12.5 cm lens was manipulated from the focal plane end. The observation hut also served as a temporary dark room during the hours of darkness. Eastman Kodak III-F plates exposed behind a Wratten 25 gelatin filter provided six exposures of the eclipse at an effective wavelength of 6300Å. Table 1 gives the mean epochs of these pictures. The last exposure was solarized since it was taken four seconds after third contact.

A single mirror coelostat fed the short focus 1.2 metre camera which used Ilford SRP emulsion sensitized to H-alpha in combination with a Wratten 25 filter. We obtained on this fine grain emulsion, a single exposure of 30 seconds duration that terminated 10 seconds ahead of third contact.

The spectroscopic experiment consisted of a twin spectrograph that examined the corona around the East and West limbs of the sun. The results obtained in this experiment have been published (Bappu, Bhattacharyya and Sivaraman 1972). All coelostats were driven by synchronous motors that operated at 115V ac, 60 Hz, generated from storage batteries.

One member of the two-man team operated the long focus camera. The narrowing crescent was centred on the image plane ten minutes before commencement of totality. Once second contact was announced he carried out the entire sequence of exposures independently. The other observer watched for the occurrence of the "flash spectrum" with the aid of an objective grating ahead of a pair of binoculars. After announcing second contact, he obtained the long spectrographic exposure planned for the West limb, and then obtained the single exposure on fine-grain emulsion with the small-focus coronal camera.

The plates were all developed at Kodaikanal a few days after the eclipse. Photometric standards with the aid of a Hilger step wedge were impressed on plates taken from the same boxes as the coronal plates. Each photograph and its calibration plate were processed together in the developer indicated in table 1.

The first plate, although exposed at the correct epoch to record the spicules, does not show them. The plate is quite dark near the limb because of development in D-19. All the five plates show a myriad of coronal fine structure. Figure 1 shows the photograph of the corona of Plate IV.

3. Photometry of the corona

The isophotes of the corona were obtained by the equidensitometry technique using the Sabbattier effect. We have employed this technique with much success for several different programmes at this Institute, including a photometric study of the solar

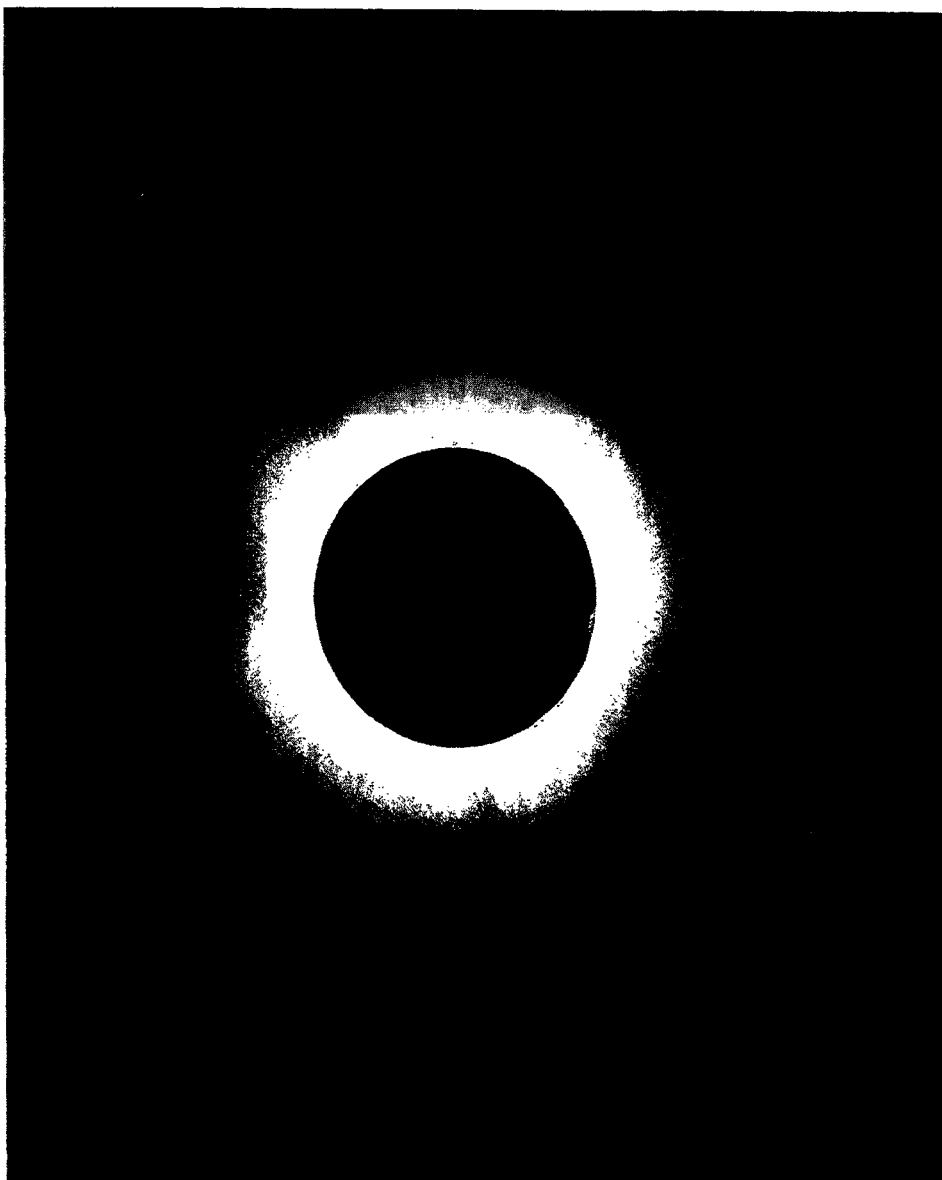


Figure 1. The solar corona of March 7, 1970, photographed by the Kodaikanal Observatory expedition at Miahuatlan, Mexico. Top is North and East is on the left.

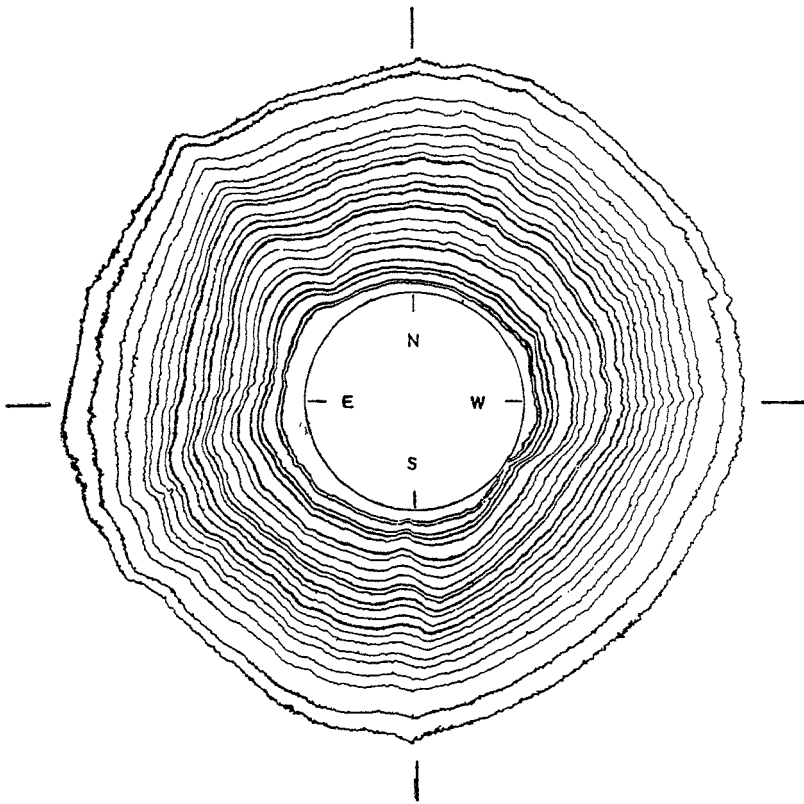


Figure 2. Isophotes of the solar corona. Isophote numbers decrease from the solar limb outwards.

corona of July 20, 1963 (Bappu and Bhatnagar 1967). This is a remarkably simple, inexpensive and accurate procedure for evaluation of contours of equal density. A final determination of the intensity levels of each density contour is easily done through conventional microphotometry.

For the present study we have used Orwo FU-5 emulsion to obtain the equidensities. Isophotes for Plates II, III, IV and V were derived separately. A final composite has been made by the combination of the family of contours of each plate. There was considerable overlap between the contours of the plates, for there were at least three in common between any pair of plates examined. The matching of the isophotes of one plate with those of another was done in such a way as to ensure perfect overlapping at these common density contours. The composite thus derived and shown in figure 2 has 23 contours running from $r=1.1$ to 3.5 , r being the distance from the sun's centre in units of the solar radius.

We next made microphotometer scans along two diameters roughly at position angles 0° , 90° , 180° and 270° . These density tracings were reduced to intensities with the aid of the calibration curve for each plate. The mean of the four values was chosen to represent the intensity level of each of the isophotes on an arbitrary scale, this scale itself being different for the four plates. The intensities derived from each plate have good accuracy since they are read off from the linear part of the calibration curve. The next step is to bring the intensities to a common scale for which we adopted that of Plate IV as the standard. Mean conversion factors are then derived from ratios of intensities

of the common isophotes, and in this way all the isophotes are brought on to a common scale. The isophote system derived from each plate also fits in with those of Plate IV which enables coverage of intensity to $r = 3.5$. Hence, it is as if the entire set of isophotes have been derived from Plate IV with the central circle in figure 2 depicting the moon. Since the epoch of this plate corresponds closely to the time of mid-totality, the derived family of equal intensity contours can be considered as representative of conditions at mid-eclipse. The system of isophotes was then transferred with their origin as the centre of the sun following the calculations of Becker (1908).

A common source of error, in general coronal photometry at eclipses is caused by scattered light. Microphotometer traces through the moon's image showed no evidence of any fog that could be ascribed to scattering in the atmosphere. These errors, if such existed, are much less than one per cent. We should expect it to be so, since the sky at Miahuatlan was exceptionally transparent on the day of the eclipse.

4. Polar and equatorial intensity gradients

For conversion of our intensity values to absolute brightness expressed in terms of the brightness of the disc, we use the results of the Russian team that also observed the eclipse from the vicinity of Miahuatlan. Our intensities agree very well with those of the Russian data (Gulyayev 1971) from $r = 1.125$ to 1.45. By a tie-up in this region, we derive absolute intensities of our isophote system in units of 10^{-10} of the average brightness of the solar disc. Table 2 gives the intensities in absolute units of the isophotes. We present in Table 3, the values of r for each isophote for all position angles at intervals of 10° referred to the centre of the solar disc. Following Baumbach (1937) and van de Hulst (1950) we can represent the observed radial brightness distribution by expressions of the form $\sum_n C_n r^{-n}$. Through successive approximations

Table 2. Intensities in the equatorial direction of the corona of March 7, 1970. Intensities are in units of 10^{-10} times the average brightness of the solar disc.

Isophote No.	r_{equator}	Intensity I	Isophote No.	r_{equator}	Intensity I
1	3.1209	13.8	13	1.8422	204.4
2	2.9206	16.5	14	1.7831	234.0
3	2.6828	22.3	15	1.7205	391.0
4	2.5754	27.0			
5	2.4502	35.9	16	1.6311	550.0
			17	1.5596	742.0
6	2.3787	42.9	18	1.5059	941.0
7	2.2929	52.3	19	1.3986	1717.0
8	2.2177	62.3	20	1.3414	2322.0
9	2.1551	72.8			
10	2.0693	90.5	21	1.2967	2958.0
			22	1.2108	6157.0
11	1.9906	118.4	23	1.1679	9254.0
12	1.9316	140.5			

Table 3. Values of r for each isophote at intervals of 10°

Isophote No.	Position Angle											
	0°	10°	20°	30°	40°	50°	60°	70°	80°	90°	100°	110°
1	3.205	3.098	3.107	3.095	3.306	3.135	3.112	3.187	3.146	3.206	3.200	3.177
2	3.101	3.019	3.018	3.016	3.199	3.028	2.976	3.001	2.960	2.980	2.992	3.005
3	2.876	2.794	2.785	2.787	3.013	2.856	2.772	2.751	2.746	2.741	2.788	2.855
4	2.751	2.686	2.667	2.676	2.895	2.760	2.665	2.618	2.620	2.615	2.681	2.730
5	2.615	2.536	2.517	2.533	2.741	2.616	2.504	2.464	2.459	2.454	2.520	2.604
6	2.536	2.464	2.446	2.454	2.666	2.556	2.450	2.393	2.388	2.383	2.466	2.486
7	2.447	2.382	2.356	2.361	2.584	2.491	2.379	2.321	2.298	2.293	2.391	2.408
8	2.350	2.293	2.267	2.283	2.512	2.427	2.300	2.239	2.209	2.222	2.316	2.336
9	2.304	2.246	2.202	2.229	2.451	2.384	2.279	2.178	2.155	2.168	2.277	2.282
10	2.178	2.139	2.102	2.122	2.333	2.295	2.164	2.089	2.055	2.068	2.162	2.182
11	2.089	2.053	2.031	2.039	2.262	2.223	2.100	2.017	1.996	2.000	2.109	2.114
12	2.028	1.996	1.956	1.986	2.172	2.169	2.053	1.964	1.923	1.954	2.062	2.050
13	1.928	1.910	1.862	1.871	2.072	2.080	1.968	1.867	1.833	1.882	2.001	1.971
14	1.874	1.856	1.820	1.818	2.019	2.026	1.932	1.821	1.787	1.846	1.965	1.918
15	1.756	1.745	1.730	1.710	1.904	1.962	1.871	1.767	1.726	1.782	1.912	1.871
16	1.660	1.645	1.648	1.610	1.797	1.865	1.789	1.677	1.637	1.703	1.812	1.764
17	1.570	1.570	1.576	1.514	1.679	1.758	1.699	1.606	1.565	1.621	1.733	1.674
18	1.509	1.506	1.516	1.460	1.625	1.694	1.653	1.559	1.529	1.578	1.669	1.603
19	1.373	1.388	1.390	1.381	1.511	1.579	1.556	1.463	1.422	1.489	1.554	1.478
20	1.302	1.320	1.319	1.306	1.421	1.508	1.485	1.409	1.386	1.417	1.483	1.424
21	1.255	1.280	1.265	1.263	1.357	1.447	1.431	1.373	1.350	1.381	1.436	1.381
22	1.183	1.195	1.186	1.192	1.285	1.311	1.295	1.266	1.261	1.263	1.304	1.263
23	1.159	1.170	1.151	1.163	1.207	1.271	1.252	1.230	1.225	1.227	1.257	1.227

(continued on page 122)

Table 3 continued

Isophote No.	Position Angle											
	120°	130°	140°	150°	160°	170°	180°	190°	200°	210°	220°	230°
1	3.162	2.953	2.953	2.971	3.076	3.092	3.139	3.014	2.943	2.891	2.894	2.897
2	3.012	2.864	2.860	2.892	2.944	2.924	2.942	2.835	2.746	2.695	2.698	2.719
3	2.833	2.667	2.645	2.656	2.712	2.692	2.674	2.620	2.532	2.498	2.494	2.486
4	2.793	2.560	2.523	2.553	2.604	2.584	2.584	2.513	2.424	2.373	2.394	2.379
5	2.593	2.434	2.402	2.445	2.479	2.459	2.459	2.413	2.317	2.265	2.258	2.261
6	2.522	2.377	2.323	2.374	2.397	2.395	2.395	2.323	2.271	2.201	2.186	2.182
7	2.432	2.291	2.234	2.302	2.307	2.280	2.280	2.227	2.138	2.094	2.090	2.075
8	2.350	2.220	2.162	2.220	2.229	2.209	2.191	2.198	2.081	2.022	2.014	2.003
9	2.289	2.166	2.098	2.152	2.157	2.137	2.101	2.101	2.013	1.961	1.929	1.914
10	2.203	2.077	2.026	2.070	2.075	2.048	2.012	2.041	1.949	1.890	1.857	1.846
11	2.117	2.016	1.947	1.984	1.996	1.966	1.923	1.966	1.881	1.818	1.786	1.767
12	2.060	1.959	1.901	1.927	1.925	1.905	1.894	1.923	1.841	1.765	1.721	1.717
13	1.974	1.884	1.822	1.819	1.835	1.815	1.772	1.840	1.752	1.675	1.632	1.617
14	1.928	1.844	1.794	1.791	1.789	1.762	1.729	1.801	1.723	1.643	1.596	1.581
15	1.874	1.791	1.751	1.741	1.717	1.686	1.654	1.737	1.655	1.568	1.542	1.520
16	1.778	1.701	1.679	1.640	1.621	1.590	1.536	1.654	1.586	1.496	1.452	1.445
17	1.670	1.594	1.593	1.544	1.517	1.493	1.493	1.547	1.509	1.425	1.374	1.359
18	1.606	1.540	1.536	1.479	1.460	1.422	1.429	1.493	1.459	1.378	1.320	1.302
19	1.463	1.415	1.393	1.340	1.342	1.314	1.314	1.340	1.341	1.282	1.213	1.323
20	1.384	1.361	1.329	1.283	1.281	1.261	1.250	1.279	1.269	1.239	1.177	1.137
21	1.345	1.315	1.286	1.236	1.220	1.225	1.214	1.232	1.226	1.203	1.142	1.102
22	1.223	1.236	1.189	1.158	1.148	1.150	1.143	1.143	1.147	1.146	1.105	1.055
23	1.187	1.200	1.143	1.122	1.113	1.114	1.107	1.111	1.112	1.106	1.070	1.055

(continued on page 123)

Table 3 continued

Isophote No.	Position Angle											
	240°	250°	260°	270°	280°	290°	300°	310°	320°	330°	340°	350°
1	2.901	2.964	3.044	3.059	3.086	3.120	3.146	3.100	3.111	3.182	3.249	3.243
2	2.723	2.745	2.858	2.898	2.943	3.016	3.003	2.971	2.982	3.050	3.131	3.143
3	2.490	2.531	2.589	2.659	2.689	2.712	2.770	2.757	2.750	2.824	2.910	2.911
4	2.390	2.423	2.518	2.559	2.582	2.629	2.663	2.649	2.639	2.710	2.802	2.803
5	2.283	2.316	2.411	2.487	2.474	2.515	2.549	2.517	2.510	2.567	2.659	2.667
6	2.211	2.245	2.339	2.416	2.398	2.433	2.448	2.435	2.439	2.477	2.570	2.582
7	2.089	2.137	2.232	2.323	2.299	2.354	2.377	2.345	2.367	2.370	2.470	2.481
8	2.025	2.066	2.175	2.255	2.231	2.283	2.305	2.266	2.295	2.298	2.391	2.392
9	1.943	1.987	2.089	2.176	2.170	2.200	2.216	2.184	2.224	2.216	2.309	2.320
10	1.864	1.916	2.024	2.094	2.099	2.139	2.144	2.113	2.135	2.109	2.194	2.177
11	1.793	1.833	1.960	2.008	2.020	2.068	2.044	2.030	2.067	2.037	2.105	2.106
12	1.721	1.776	1.928	1.951	1.941	2.004	1.980	1.952	2.009	1.966	2.015	2.034
13	1.614	1.672	1.785	1.825	1.830	1.889	1.858	1.869	1.902	1.855	1.908	1.909
14	1.585	1.644	1.749	1.790	1.784	1.835	1.823	1.827	1.866	1.808	1.844	1.873
15	1.517	1.558	1.659	1.682	1.687	1.728	1.715	1.719	1.730	1.708	1.747	1.748
16	1.428	1.493	1.570	1.593	1.598	1.639	1.636	1.648	1.652	1.619	1.640	1.659
17	1.335	1.422	1.516	1.521	1.526	1.549	1.554	1.576	1.562	1.547	1.557	1.551
18	1.270	1.386	1.463	1.468	1.469	1.485	1.501	1.512	1.509	1.490	1.479	1.480
19	1.192	1.297	1.345	1.342	1.347	1.352	1.393	1.361	1.373	1.368	1.354	1.355
20	1.159	1.250	1.284	1.289	1.276	1.288	1.350	1.308	1.312	1.297	1.289	1.290
21	1.131	1.207	1.237	1.242	1.229	1.245	1.304	1.243	1.247	1.233	1.246	1.212
22	1.095	1.168	1.194	1.182	1.169	1.184	1.214	1.175	1.169	1.165	1.182	1.176
23	1.077	1.125	1.169	1.142	1.140	1.163	1.178	1.136	1.133	1.136	1.150	1.140

and the method of least squares we obtain for distributions along equatorial and polar radii,

$$I_{\text{equator}} = \frac{62185 \cdot 27}{r^{17.0}} + \frac{13949 \cdot 6}{r^{7.0}} + \frac{164 \cdot 4}{r^{3.0}}$$

$$I_{\text{pole}} = \frac{25910 \cdot 1}{r^{19.0}} + \frac{6320 \cdot 4}{r^{6.9}} + \frac{515 \cdot 6}{r^{4.5}}$$

Figure 3 depicts the equatorial expression along with the observed points and the van de Hulst curves for the corona at both sunspot maximum and minimum. In figure 4, the van de Hulst formulation for the polar intensity distribution is also plotted along with our expression as well as the observed values of I . It is difficult to reconcile the observed points with the van de Hulst parameters.

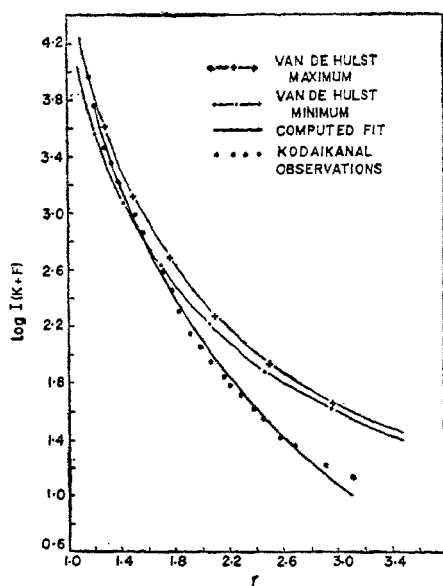


Figure 3. Coronal intensities (K+F) along the equatorial diameter. r is the distance from the sun's centre in units of the sun's radius.

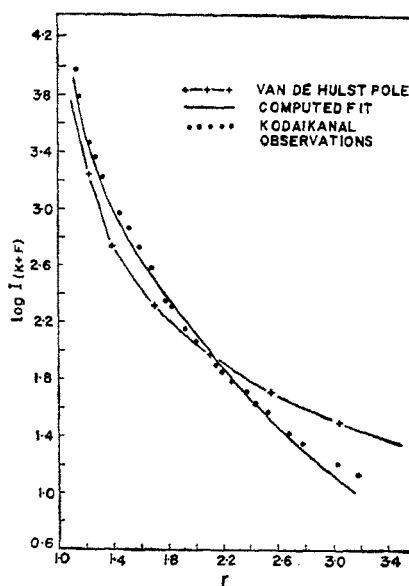


Figure 4. Coronal intensities (K+F) along the polar diameter.

5. Intensity gradients in the streamers and gaps

Bohlin *et al* (1971) have made photometric observations of the outer corona from $3R_{\odot}$ to $8R_{\odot}$ from a rocket mounted coronagraph. We have transformed their observations to our unit of brightness and plotted them in figure 5 along with our values of the inner regions of the corona. Notice the very good fit in the region of overlap around $3 \cdot 2R_{\odot}$. The curve of figure 5 thus represents the radial variation along the equator of coronal brightness from $r = 1 \cdot 1$ to $8 \cdot 0$.

Our data can be utilized easily for a study of radial gradients in the different streamers and gaps. Figure 6 is a plot of observed intensities in five conspicuous streamers observed at this eclipse. The inset in figure 6 is a sketch of streamers from a composite of Newkirk's radial neutral density photograph and the rocket version of the outer corona obtained by Bohlin *et al* (1971). Figure 7 depicts the intensity distribution for

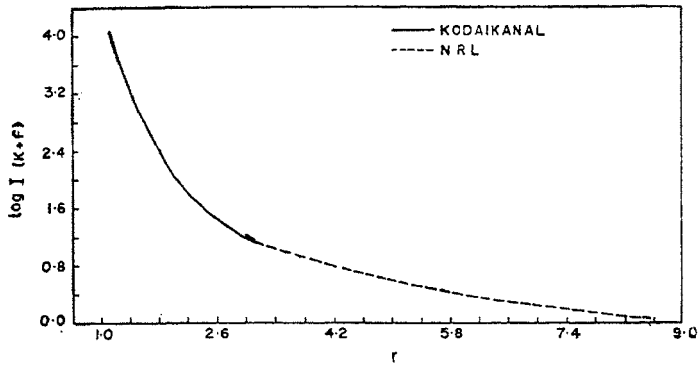


Figure 5. Equatorial intensity from $r=1.1$ to 8.0

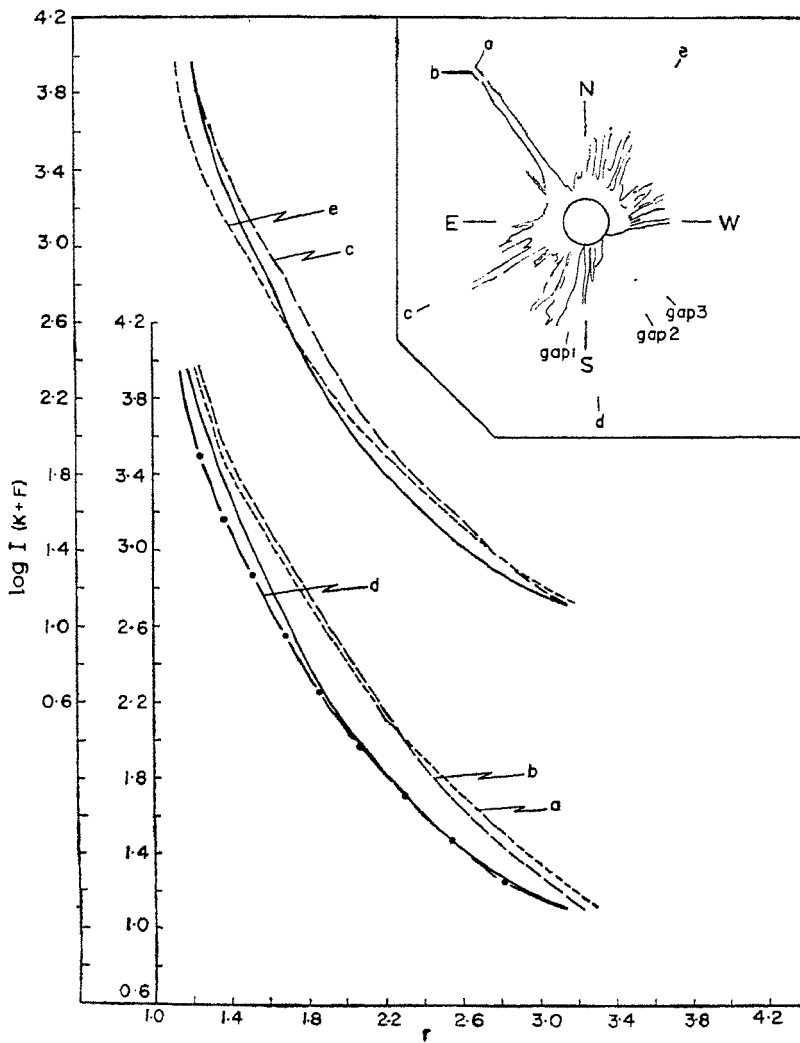


Figure 6. Radial intensity distribution along streamers. The location of the streamers a, b, c, d, e can be seen in the inset sketch of the corona. The continuous curve is the equatorial intensity shown for comparison.

7. The ellipticity of the corona

The Ludendorff parameter which is a measure of the ellipticity or the flattening of the isophotes is defined by the formula

$$\epsilon = \frac{d_{\text{equator}}}{d_{\text{pole}}} - 1$$

where d_{equator} is the mean value of the diameters of an isophote along the equator and in two directions making an angle of 22.5° with it. In a similar way d_{pole} is the average diameter along the pole and 22.5° on either side. Table 5 gives the value of ϵ for the different isophotes and figure 9 shows the variation of ϵ with the position angle. The ellipticity values are low as is to be expected from a corona at solar maximum, and especially around $2R_\odot$ circular symmetry prevails. Waldmeier (1971) also finds the ellipticity to be zero for this corona.

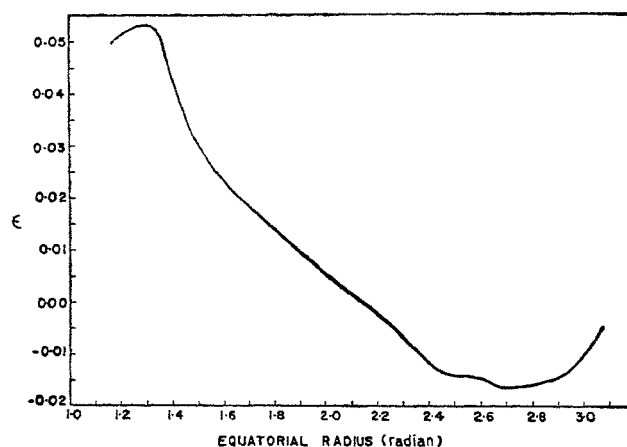


Figure 9. The flattening parameter ϵ as a function of the position angle.

Acknowledgements

Preparation for an expedition to a distant location is possible only by the combined effort of several individuals. We are particularly indebted to Messrs A P Jayarajan, K C A Raheem, P M Nayar, L Peter and Iqbal Ali, for their wholehearted co-operation. To Drs A Poveda and M Méndez of the University of Mexico our grateful thanks are due for their hospitality and all the help they provided in Mexico. The Indian Ambassador, Mr Masand, and the officers of the Embassy contributed much towards the successful accomplishment of the expedition.

References

- Bappu M K V and Bhatnagar A 1967 *Kodaikanal Observ. Bull. Ser. A* No. 190
- Bappu M K V, Bhattacharyya J C and Sivaraman K R 1972 *Solar Phys.* **26** 366
- Baumbach S 1937 *Astron. Nachr.* **263** 121
- Becker L 1908 *Mem. Roy. Astron. Soc.* **57** 307
- Bohlin J D, Koomen M J and Tousey R 1971 *Solar Phys.*, **21** 408
- Gulyaev R A 1971 *Russian Solar Data* No. 6 p 80
- van de Hulst H C 1950 *Bull. Astron. Inst. Neth.* **11** 135
- Waldmeier M 1970 *Nature, London* **226** 1139
- Waldmeier M 1971 *Physics of the Solar Corona* (Reidel Publ. Co., Dordrecht-Holland) p. 130
- Wallenquist A 1956 *Ann. Observ. Uppsala*, **4** No. 4